

1 **Structural basis for intrinsic transcription termination**

2 Linlin You^{1,2}, Expery Omollo³, Chengzhi Yu^{1,2}, Rachel A. Mooney³, Jing Shi^{4,5}, Liqiang
3 Shen^{1,2}, Xiaoxian Wu^{1,2}, Aijia Wen⁴, Dingwei He^{1,2}, Yuan Zeng^{1,2}, Yu Feng^{4,*}, Robert
4 Landick^{3,*}, Yu Zhang^{1,*}

5

6

7

8

9

10

11

12

13

14

15

16 ¹Key Laboratory of Synthetic Biology, CAS Center for Excellence in Molecular Plant Sciences,
17 Shanghai Institute of Plant Physiology and Ecology, Chinese Academy of Sciences; Shanghai
18 200032, China

19 ²University of Chinese Academy of Sciences; Beijing 100049, China

20 ³Department of Biochemistry and Department of Bacteriology, University of Wisconsin-
21 Madison, Madison, Wisconsin 53706, USA

22 ⁴Department of Biophysics, and Department of Pathology of Sir Run Run Shaw Hospital,
23 Zhejiang University School of Medicine; Hangzhou 310058, China

24 ⁵Department of Pathogen Biology, School of Medicine & Holistic Integrative Medicine,
25 Nanjing University of Chinese Medicine, Nanjing, China.

26

27

28 *Corresponding authors. Email: yzhang@cemps.ac.cn (Y.Z.), rlandick@wisc.edu (R.L.),
29 yufengjay@zju.edu.cn

30

31

32

33 **Abstract**

34 Efficient and accurate termination is required for gene transcription in all living organisms.
35 Cellular RNA polymerases (RNAP) in both bacteria and eukaryotes can terminate their
36 transcription through a factor-independent termination pathway (called intrinsic termination
37 transcription in bacteria), in which RNAP recognizes terminator sequences, stops nucleotide
38 addition, and releases nascent RNA spontaneously. Here we report a set of single-particle
39 cryo-EM structures of *E. coli* transcription intrinsic termination complexes representing key
40 intermediate states of the event. The structures show how RNAP pauses at terminator
41 sequences, how the terminator RNA hairpin folds inside RNAP, and how RNAP rewinds the
42 transcription bubble to release RNA and then DNA. These macromolecular snapshots define a
43 structural mechanism for bacterial intrinsic termination and a pathway for RNA release and
44 DNA collapse relevant for factor-independent termination by all RNA polymerases.

45

46 Genomic DNA is composed of functional genes transcribed to RNAs with defined 5' and 3'
47 boundaries. The 5' boundary is defined by a promoter, from which RNAP initiates RNA
48 synthesis¹. The 3' boundary is defined by a terminator, at which RNAP stops transcription and
49 releases the nascent RNA²⁻⁵. Efficient and accurate termination is required for gene
50 transcription in all living organisms to ensure precise control of transcription units and to
51 define the 3' boundary of RNA transcripts^{3,4}. Programmed transcription termination of RNAP
52 occurs by two pathways, factor-independent (or intrinsic) and factor-dependent termination.
53 Intrinsic termination requires only interactions of RNA and DNA with RNAP and can be
54 modulated by transcription factors⁵⁻⁸. Intrinsic termination is prevalent in viruses and bacteria
55 and used in eukaryotes by RNAPIII^{6,8,9}.

56
57 The intrinsic terminator sequences in bacteria comprise a G/C-rich inverted repeat
58 immediately followed by a stretch of thymidine that encodes an RNA with a G/C-rich
59 terminator hairpin immediately followed by a uridine tract^{10,11}. Genetic, biochemical, and
60 single-molecule studies all suggest that intrinsic termination occurs via three sequential
61 intermediates: (i) a pause state when RNAP pauses at the terminator; (ii) a hairpin-nucleation
62 state when the RNA hairpin partially folds into RNAP; and (iii) a hairpin-completion state
63 when the RNA hairpin completes folding and releases nascent RNA aided by the weak rU–dA
64 base pairs. However, how the compact terminator sequence pauses, destabilizes, and
65 dissociates RNAP remains elusive. To address the questions, we determined a set of cryo-EM
66 structures representing the key intermediate states formed during intrinsic termination.

67
68 **RNAP pauses at the terminator sequence by adopting a half-swiveled conformation**
69 RNAP first pauses at the -2/-1 positions (-1 corresponds to the position of the RNA 3' end)
70 of intrinsic terminators to begin intrinsic termination^{8,12}. To study the structural mechanism of
71 the terminator-induced pause, we reconstituted a paused transcription termination complex
72 (TTC-pause) using *E. coli* RNAP core enzyme and a nucleic-acid scaffold that comprises a
73 nascent RNA with λt_{R2} terminator sequence but lacking the upstream half of the hairpin stem

74 (Fig. 1A). The TTC-pause structure was determined at 3.6-Å resolution using single-particle
75 cryo-EM (Fig. S1 and Table S2). The cryo-EM map of TTC-pause shows unambiguous
76 signals for ribonucleotides and deoxyribonucleotides within and near the transcription bubble,
77 including the 10-bp RNA–DNA hybrid, the 10-nt single-stranded non-template DNA
78 (ntDNA), the 12-bp downstream double-stranded (dsDNA), and 3-bp of the upstream dsDNA
79 (Figs. 1B and 1C, and Movie S1).

80
81 The RNA–DNA hybrid of TTC-pause adopts a half-translocated state, an off-pathway state
82 that has been reported previously in paused transcription complexes^{13–15}. In the half-
83 translocated state, the RNA strand has translocated by 1-nt step from the pre-translocation
84 state but the next template strand DNA (tDNA) nucleotide remains base-paired in the
85 downstream dsDNA (Figs. 1D and S2C, and Movie S1). This bp is unwound and
86 untranslocated except for slight positional shift of backbone phosphates (Fig. S2C). Half-
87 translocation results in a tilted RNA–DNA hybrid and an empty NTP-binding site (i+1 site)
88 lacking the template nucleotide for base-pairing to the incoming NTP (Fig. 1D). A survey of
89 100 native intrinsic terminators shows that intrinsic terminators resemble the consensus
90 sequence for elemental pausing at two out of the three key positions (S₋₁₀U₋₁ vs. S₋₁₀Y₋₁G₊₁;
91 Figs. 1E, S2A, and S2B)^{11,16,17}. We infer that the sequences at the upstream and downstream
92 edges of the transcription bubble (S₋₁₀, U₋₁) likely account for formation of the half-
93 translocated conformation of TTC-pause complex⁵.

94
95 We also observed a global conformational change of RNAP involving multiple structural
96 modules in TTC-pause compared with the normal transcription elongation complex (EC)¹⁸.
97 The clamp module of RNAP rotates along an axis parallel to the bridge helix. The rotation
98 movement of clamp module resembles the ‘swivel’ movement observed in the hairpin-
99 stabilized paused elongation complex (PEC)^{13,14,19}, but it only reaches halfway to the fully
100 swiveled position (Fig. 1F). However, different from the swivel movement in the hairpin-
101 stabilized PEC complex, the RNAP-β lobe/SII module in TTC-pause moves slightly towards

102 the RNAP main cleft, likely due to unique interactions between RNAP and ntDNA of the
103 transcription bubble (Fig. 1G and Movie S1). These movements of structural modules in
104 TTC-pause likely accommodate the slightly shifted downstream dsDNA in the downstream
105 dsDNA channel and stabilize the half-translocated RNA–DNA hybrid in the main cleft (Figs.
106 S2C and S2D).

107

108 Our cryo-EM map of TTC-pause revealed a novel path of the single-stranded ntDNA in the
109 transcription bubble across the RNAP main cleft. The ntDNA was accommodated in the upper
110 floor of the main cleft and was separated from the active-site tunnel by the RNAP- β' rudder
111 loop and fork loop 2 (Figs. 1C and S2E). Eight nucleotides of the ntDNA form a continuous
112 base stack that starts upstream at the RNAP- β' coiled-coil (Fig. 1G and S2E), travels across
113 the cleft to the RNAP- β protrusion and lobe, and follows fork loop 2 to reach the downstream
114 dsDNA (Fig. S2E). The –4A is flipped out \sim 180° from this continuous base stack. The
115 backbone phosphates of the stacked nucleotides are stabilized by polar contacts with RNAP
116 residues β' R271, β' R297, β R470, and β R473 (Fig. S2F). Residue β W183 supports the 8-nt
117 base stack and separates it from the downstream dsDNA (Fig. S2F).

118

119 The interaction between RNAP and the –4 nucleotide is notable. The flipped out –4
120 nucleotide inserts into a protein pocket (NT–4 pocket) located in the gap between RNAP β
121 protrusion and lobe (Fig. 1G). The A–4 base was sandwiched between residues β R180 and
122 β V469; and the N1 atom of the adenine moiety makes a H-bond with β R465 (Figs. 1G and
123 S2F). To test for potential effects of the pocket interaction on intrinsic termination, we
124 measured the termination efficiency of RNAP derivatives bearing substitutions in the pocket
125 at three different terminators. The results revealed no obvious effects on termination
126 efficiency of disruption of either the stacking interaction (β R180A/ β V469A) or H-bond
127 interaction (β R465A) (Figs. S3A-F). Disruption of the pocket interaction also had no effect
128 on transcriptional pausing at a hairpin-less λ P_R terminator (Fig. S3G). Although no significant

129 role in intrinsic termination was found, the pocket interaction also has been observed in a
130 promoter escape complex and thus could play roles in other stages of transcription²⁰.

131

132 **RNA hairpin nucleation in the RNA exit channel prepares the TTC for transcription**
133 **bubble rewinding**

134 The RNA hairpin of intrinsic terminators starts to fold in the RNA exit channel after RNAP
135 pauses at terminators, a stage named hairpin nucleation^{12,21}. To trap the hairpin-nucleation
136 complex of transcription termination (TTC-hairpin), we incubated the TTC-pause complex
137 with an antisense RNA10 (asRNA10) to form a 10-bp RNA duplex with the nascent RNA that
138 mimics the hairpin stem (-20 to -11) and determined a TTC-hairpin structure at 3.1 Å
139 resolution (Figs. 2A and S4, and Table S2). The cryo-EM map of TTC-hairpin revealed clear
140 and sharp signals for the transcription bubble. The RNA–DNA hybrid adopts the same half-
141 translocated conformation as in TTC-pause and the ntDNA nucleotides stack together and
142 make interactions with RNAP essentially the same as in TTC-pause (Figs. 2C and S5A). The
143 cryo-EM map of TTC-hairpin shows unambiguous signal for the 14-bp downstream dsDNA,
144 the 3-bp upstream dsDNA, and, most importantly, the 10-bp dsRNA in the RNA exit channel
145 (Figs. 2B and 2C, and Movie S2). These features indicate we successfully trapped the TTC-
146 hairpin complex of intrinsic termination.

147

148 The 10-bp dsRNA was tightly accommodated in the RNA exit channel by RNAP β' dock, β'
149 C-terminal helix (β' CTH), β' zinc-binding domain (β' ZBD), and β flap (Fig. 2D), consistent
150 with the important roles of these elements in intrinsic termination^{22,23}. The phosphate
151 backbones of the RNA hairpin were held by RNAP polar residues in the RNA exit channel,
152 including $\beta'K66$, $\beta'K76$, $\beta'R77$, $\beta'Q1256$, $\beta'K395$, $\beta'K398$, $\beta N856$, $\beta K890$, $\beta K914$, and
153 $\beta R919$ (Fig. 2E). The innermost base pair of the RNA duplex reaches the bottom of the RNA
154 exit channel. The -11G of the nascent RNA makes a base-stack interaction with $\beta L1253$ and
155 the sugar moiety of the asRNA -11C fits into a shallow pocket of β' ZBD (Fig. 2F). A

156 positively charged groove likely guides ssRNA upstream of hairpin stem out of the RNA exit
157 channel (Fig. S5B). Further extension of the RNA hairpin stem was stopped by β Sw3, β'
158 ZBD, and β' lid (Fig. 2G). Most of these features of the hairpin stem closely match those
159 observed for the hairpin-stabilized *hisPEC* even though the TTC-hairpin stem is extended 1
160 bp closer to the RNA–DNA hybrid^{13,14}.

161

162 The formation of an RNA duplex in TTC-hairpin causes a global conformational change of
163 RNAP. The RNA duplex enlarges the RNA exit channel by stretching the four surrounding
164 structural elements (Fig. 2H), likely triggering a global conformational change of RNAP
165 structure modules, including further swiveling of the clamp module and outward rotation of
166 the protrusion/lobe/SI1 module (Fig. 2I and Movie S2). The net result of such global
167 rearrangement widens the main cleft and secures the hairpin in the RNA exit channel.
168 Moreover, the fully swiveled conformation prevents trigger loop from refolding and further
169 stabilizes the half-translocated RNA-DNA hybrid^{13,24}. In short, our TTC-hairpin structure
170 show that the RNA duplex in the RNA exit channel induces further conformational changes of
171 RNAP compared with TTC-pause to stabilize the pause and likely to prepare for subsequent
172 completion of RNA hairpin.

173

174 The completion of RNA hairpin requires melting of at least two upstream base pairs of RNA-
175 DNA hybrid²⁵. Our cryo-EM structure of TTC-hairpin provides a structural clue for how the
176 first base pair of the RNA–DNA hybrid is disrupted. In the TTC-hairpin structure, the half-
177 translocated RNA–DNA hybrid shifts each of template nucleotide towards upstream from
178 their respective positions in the pre-translocation state (Fig. 2J). As a result, the –10
179 nucleotide of tDNA shifts ~1-bp register out of the RNAP active-center cleft to a new position
180 under the small tunnel formed by the rudder and lid loops (Figs. 2K, S5C, and S5D). This
181 new location allows unpairing of tDNA with the –10 nucleotide of the nascent RNA and its
182 flipping through the tunnel to pair with the –10 nucleotide of ntDNA (Fig. S5E and Movie

183 S3). Rewinding of this upstream base pair of the transcription bubble would weaken the next
184 base-pair in the RNA–DNA hybrid due to loss of stacking interactions, thus enabling its
185 disruption and lowering the energy barrier to RNA hairpin completion. The base pair at the
186 –10 position shows the weakest map signals among the nucleotides of the RNA–DNA hybrid
187 (Fig. S5F), indicative of its high flexibility necessary for spontaneous unwinding.

188

189 **Rewinding of transcription bubble promotes RNA release**

190 The last stage of transcription termination involves disruption of RNA–DNA hybrid,
191 completion of RNA hairpin, rewinding of transcription bubble, and release of RNA and
192 DNA^{8,12,25–28}. To trap intermediates of the last stage of intrinsic termination, we took
193 advantage of asRNA-induced termination (Fig. 3A)⁸. The in vitro transcription termination
194 assay suggests that, upon asRNA challenge, RNAP began to release nascent RNA in 30
195 seconds and released most of the nascent RNA at 5 minutes (Fig. 3B). Therefore, we
196 challenged the TTC-pause complex with excess amount of 12-nt asRNA and vitrified the
197 reaction mixture after 3-minute incubation, followed by cryo-EM data collection. A cryo-EM
198 map was reconstructed at 3.5 Å from 54,471 particles (19% of total particles) after two
199 rounds of 3D classification (Fig. S6 and Table S2). The cryo-EM density map for this novel
200 complex (TTC-release) shows clear signals for 14-bp dsDNA in the downstream DNA
201 channel, 6-bp upstream dsDNA located between the β' clamp helices and β protrusion, and a
202 partially rewound transcription bubble evidenced by the 5-nt single-stranded ntDNA (Figs. 3C
203 and 3D, and Movie S4). The cryo-EM map shows no signal in the RNA-exit channel and
204 weak disconnected signal in the active-center cleft that is likely from the non-specific
205 rebinding of released RNA (Fig. 3D)²⁹. The map features suggest that we have trapped an
206 intermediate state of DNA–RNA release (TTC-release), in which RNA is released from the
207 RNA exit channel, the transcription bubble is disrupted, and the ntDNA and tDNA of the
208 transition bubble are partially rewound (Fig. 3E and Movie S4).

209

210 The upstream dsDNA of TTC-release undergoes a radical conformation change compared
211 with that of TTC-hairpin. The helix axis of the upstream dsDNA of TTC-release rotates ~75°
212 in an upward direction compared with that of TTC-hairpin (Fig. S7A). The rotation of the
213 dsDNA relocates the 6-bp upstream dsDNA (−17 to −12) away from RNAP and thus becomes
214 disordered in the structure (Fig. S7B). The rewound 5-bp dsDNA (−10 to −6) were loosely
215 restrained by β protrusion, β' CC, and β' rudder (Fig. 3F). Further rewinding of the upstream
216 dsDNA is stopped by the β lobe domain and requires cleft opening to a greater extent (Fig.
217 3F). The 5-nt single-stranded ntDNA remains in the same location as in TTC-pause and TTC-
218 hairpin (Fig. 3E). The 14-bp dsDNA of TTC-release locates at the downstream dsDNA
219 channel and makes interactions with RNAP as it does in an EC (Fig. S7C). Structural
220 comparison shows that the RNAP clamp and lobe adopt the closed conformation seen in
221 canonical EC (Fig. S7D), consistent with the previous findings that clamp opening is required
222 for DNA release³⁰. In short, our TTC-release structure suggests that DNA duplex remains
223 bound to RNAP in a partially rewound form after RNA release.

224

225 The TTC-release complex also shows that transcription bubble rewinding is accompanied by
226 hairpin completion and release of the nascent RNA^{31,32}. The structure of the TTC-hairpin
227 complex reveals the −10 nucleotide of tDNA is ready to unpair with RNA and to rewind with
228 the −10 nucleotide of ntDNA (Figs. 2J, 2K and S5C-E). These results lead us to hypothesize
229 that rewinding of the transcription bubble triggers the subsequent steps of hairpin completion
230 and RNA release. To test our hypothesis, we measured termination efficiency at λ_{iR2} with pre-
231 melted regions at various positions close to the termination site (Figs. 3G and S8A). The
232 results show that pre-melting the downstream half of the transcription bubble (−5 to −1; D5)
233 has no effect on the termination at all, but pre-melting the upstream half of the transcription
234 bubble (−10 to −6; U5) completely abolished termination (Fig. 3G). This result supports the
235 ideas that rewinding of transcription bubble is required for intrinsic termination and that the
236 process initiates from the upstream end, consistent with a previous report³². We next

237 performed a more refined mapping to define the minimal requirements of bubble rewinding
238 for efficient termination. Pre-melting two base pairs in the middle of the transcription bubble
239 ($-7/-6$) had little effect. Moving the 2-bp pre-melted region upstream gradually decreased the
240 termination efficiency. Strikingly, pre-melting the first two base pairs ($-10/-9$) completely
241 abolished termination, highlighting the crucial role of rewinding the first two base pairs
242 ($-10/-9$) during intrinsic termination (Fig. 3G). The same results were obtained using the ϕt_{500}
243 terminator sequence (Fig. S8B). These results support our hypothesis that rewinding the
244 transcription bubble is an important step for intrinsic termination, likely through reducing the
245 energetic barriers for hairpin completion and RNA release. We also noticed that termination
246 occurred, albeit with low efficiency, in response to asRNAs (asRNA -11 and -10) that only
247 form a duplex in the RNA exit channel and do not disrupt the RNA–DNA hybrid (Fig. S8C)³³.
248 This result suggests that rewinding the transcription bubble is sufficient to induce termination
249 even without hairpin extension, consistent with bubble rewinding beginning the RNA release
250 process. Together, our cryo-EM structures and in vitro transcription results suggest that
251 rewinding the upstream two base pairs of transcription bubble is a requisite for subsequent
252 RNA hairpin completion and RNA release.

253
254 An intriguing implication of our structures is that the nascent RNA dissociates before RNAP
255 releases dsDNA, consistent with evidence that terminated RNAP can remain associated with
256 and slide on DNA after termination^{34,35}. We tested this idea by measuring the rates of RNA
257 and DNA release from TTC in physiologically relevant solutes using a scaffold that provided
258 all RNAP–DNA contacts (Fig. 3H). After addition of asRNA to trigger termination, RNA was
259 released ~ 5 times faster than DNA. This result indicates that the post-termination, the binary
260 RNAP–DNA complex survives after RNA release. This binary complex may dissociate more
261 slowly *in vivo* where sliding RNAP would not immediately encounter a DNA end.

262

263 **Discussion**

264 On the basis of our cryo-EM structures and biochemical evidence, we propose a detailed
265 model for bacterial intrinsic termination (Fig. 4 and S9): (i) RNAP pauses at the terminator
266 site containing elemental pause-like sequence motif (S₋₁₀U₋₁), where it adopts the ‘half-
267 swiveled’ conformation that accommodates a half-translocated RNA-DNA hybrid in the
268 active-site cleft; (ii) initial folding of terminator hairpin enlarges the RNA exit channel,
269 induces a ‘full-swivel’ RNAP conformation, and weakens the upstream RNA–DNA base-pair
270 interactions; (iii) RNAP rewinds the two base pairs of the upstream transcription bubble and
271 clears the energetic barrier for subsequent RNA hairpin completion; (iv) the terminator
272 hairpin completes formation in the RNA exit channel by pulling the RNA out the exit channel
273 either by ‘hybrid shearing’ (RNA moves but tDNA does not) or by pulling the RNA–DNA
274 hybrid upstream by ‘forward translocation’(the downstream duplex melts without nucleotide
275 addition to RNA) (Fig. S9)^{26,27}, meanwhile, rewinding of the transcription bubble propagates
276 along with the RNA translocation; and (v) RNAP releases the nascent RNA but retains the
277 partially rewound DNA^{34,35}. RNAP may either slide on genomic DNA or finally dissociate
278 DNA spontaneously or aided by pro-termination factors^{5,34-38}.

279

280 In summary, our cryo-EM structures of transcription termination complexes reveal how
281 bacterial RNAP pauses at intrinsic terminator sequence, how a terminator hairpin nucleates its
282 folding in the RNA exit channel to weaken the RNA–DNA hybrid, how RNAP rewinds the
283 transcription bubble to allow completion of the terminator hairpin and release of nascent
284 RNA, and how RNAP retains the partially rewound dsDNA. The structures provide structural
285 mechanisms for bacterial intrinsic termination. The “DNA rewinding-triggered RNA release”
286 mechanism provides clues for factor-independent termination at hairpin-less terminator
287 sequences by eukaryotic RNA polymerase III^{39,40}.

288

289 **Methods**

290 **Plasmid construction**

291 Plasmid pET-28a-TEV-*Ec*- σ ⁷⁰ (Table S1) was constructed by inserting the *E. coli* σ ⁷⁰ gene
292 amplified from *E. coli* genomic DNA into a modified pET-28a plasmid carrying the TEV
293 protease cleavage site by a homogenous recombination method (pEASY®-Basic Seamless
294 Cloning and Assembly Kit, Transgen Biotech, Inc.). Derivatives of pRL706 were constructed
295 by primer-mediated, site-directed mutagenesis using NEB Q5 site-directed mutagenesis
296 reagents.

297

298 ***E. coli* RNAP core enzyme**

299 *E. coli* RNAP core enzyme for cryo-EM and most *in vitro* assays was over-expressed from *E.*
300 *coli* BL21(DE3) (Novo protein, Inc.) carrying pEcABC and pCDF-*Ec* rpoZ (Table S1) and
301 purified as described⁴¹. *E. coli* RNAP core enzyme used in experiments shown in Figs. 3H
302 and S8C was purified as described previously⁴².

303 *E. coli* RNAP core enzyme with substitutions in the β subunit used in experiments shown in
304 Fig. S3 was purified using β -subunit overexpression from pRL706 derivatives (Table S1).
305 Each plasmid was independently transformed into *E. coli* strain RL1204 (Table S1) and a
306 single colony was inoculated into 30 mL LB + 100 μ g carbenicillin/mL and grown overnight
307 at 37 °C. The saturated cell culture was added to 1 L fresh LB + 100 μ g carbenicillin/mL and
308 grown at 37 °C with adequate aeration by orbital shaking in a Fernbach flask until apparent
309 OD₆₀₀ reached 0.2. β subunit overexpression was induced by adding IPTG (Gold
310 Biotechnology) to 1 mM and cell growth was monitored until apparent OD₆₀₀ reached 0.9.
311 The cells were harvested and homogenized by sonication in 30 mL Lysis Buffer (50 mM Tris-
312 HCl, pH 7.9, 5% v/v glycerol, 233 mM NaCl, 2 mM EDTA, 10 mM β -mercaptoethanol, 100
313 μ g PMSF/mL, 1 tablet of protease inhibitor cocktail (Roche), and 10 mM DTT). After
314 removing cell debris by centrifugation (27000 \times g, 15 min, 4 °C), DNA binding proteins
315 including target RNAPs were precipitated by addition of polyethyleneimine (PEI, Sigma-
316 Aldrich) to 0.6% (w/v) final and stirred for at least 10 min. After centrifugation (11000 \times g,
317 15 min, 4 °C), the protein pellet was resuspended in 25 mL of PEI wash buffer (10 mM Tris-
318 HCl, pH 7.9, 5% v/v glycerol, 0.1 mM EDTA, 5 μ M ZnCl₂, 500 mM NaCl) to remove non-
319 target proteins. After centrifugation (11000 \times g, 15 min, 4 °C), RNAP was eluted from the
320 pellet into 25 mL PEI Elution Buffer (10 mM Tris-HCl, pH 7.9, 5% v/v glycerol, 0.1 mM
321 EDTA, 5 μ M ZnCl₂, 1 M NaCl). The crude extract of RNAP was subjected to sequential
322 FPLC purifications using Ni²⁺-affinity (HisTrap FF 5 mL, Cytiva), followed by purification
323 using a Heparin column (HiTrap FF 5 mL, Cytiva). The purified RNAPs were dialyzed into
324 RNAP Storage Buffer (10 mM Tris-HCl, 25% v/v glycerol, 100 mM NaCl, 100 μ M EDTA,
325 1 mM MgCl₂, 20 μ M ZnCl₂, 10 mM DTT). Samples were aliquoted, flash frozen in
326 liquid nitrogen and stored in –80 °C.

327

328 ***E. coli* σ ⁷⁰**

329 *E. coli* σ ⁷⁰ was over-expressed in *E. coli* BL21(DE3) cells (Novo protein, Inc.) carrying
330 pET28a-TEV-*Ec*- σ ⁷⁰ (Table S1). Protein expression was induced with 0.3 mM IPTG at 18 °C
331 for 14 h when OD₆₀₀ reached to 0.6-0.8. Cell pellet was lysed in lysis buffer B (50 mM Tris-
332 HCl, pH 7.7, 500 mM NaCl, 5% (v/v) glycerol, 5 mM β -mercaptoethanol, and 0.1 mM
333 PMSF) using an Avestin EmulsiFlex-C3 cell disrupter (Avestin, Inc.). The lysate was
334 centrifuged (16,000 \times g; 50 min; 4 °C) and the supernatant was loaded on to a 2 mL column
335 packed with Ni-NTA agarose beads (Smart-Lifesciences, Inc.). The bound proteins were
336 washed by lysis buffer B containing 20 mM imidazole and eluted with the lysis buffer B
337 containing 400 mM imidazole. The eluted fractions were supplemented with TEV protease
338 and transferred to a dialysis bag to exchange buffer to 20 mM Tris-HCl, pH 7.7, 150 mM
339 NaCl, 5% (v/v) glycerol, 5 mM β -mercaptoethanol. The sample was reloaded onto the Ni-
340 NTA column, and the tag-free protein was retrieved from the flow-through fraction. The
341 sample was diluted, loaded onto a Q HP column (HiPrep Q HP 16/10, Cytiva) and eluted with

342 a salt gradient of buffer A (50 mM Tris-HCl, pH 7.7, 150 mM NaCl, 5% (v/v) glycerol, 1 mM
343 DTT) and buffer B (50 mM Tris-HCl, pH 7.7, 500 mM NaCl, 5% (v/v) glycerol, 1 mM DTT).
344 The fractions containing target proteins were collected, concentrated to 5.2 mg/mL, and
345 stored at -80 °C.

346 *E. coli* σ^{70} used in experiments shown in Figs. S3 and S8C was purified as described
347 previously⁴².

348

349 ***E. coli* RNAP holoenzyme**

350 *E. coli* RNAP core (3 μ M, final concentration) and σ^{70} (12 μ M, final concentration) were
351 incubated in 0.5 mL 20 mM Tris-HCl, pH 7.7, 100 mM NaCl, 1% (v/v) glycerol, 1 mM DTT
352 for 2 h at 4 °C. The reaction mixture was applied to a Superdex 200 10/300 column (Cytiva)
353 equilibrated in 20 mM Tris-HCl, pH 7.7, 100 mM NaCl, 1% (v/v) glycerol, 1 mM DTT.
354 Fractions containing RNAP holoenzyme were collected and concentrated to ~5 mg/mL, and
355 stored at -80 °C.

356

357 **Nucleic-acid scaffolds.**

358 Nucleic-acid scaffolds (Table S1) for cryo-EM study of *E. coli* TTC-pause and TTC-hairpin
359 were prepared as follows: nontemplate-strand DNA (5'-GGCGTACGGAAAAATAACACG
360 GCGAATACCC-3'; 0.3 mM, final concentration; Sangon Biotech), template-strand DNA (5'-
361 GGGTATTGCGCGTGAATAAAAAGGGTACGCC-3'; 0.33 mM, final concentration;
362 Sangon Biotech) and RNA (5'- GCGUCGCAGGCCUUUUAUU-3'; 0.39 mM, final
363 concentration; GenScript Biotech Corp.) in 50 μ L annealing buffer (5 mM Tris-HCl, pH 8.0,
364 200 mM NaCl, and 10 mM MgCl₂) were heated for 5 min at 95°C, cooled to 22 °C in 2 °C
365 steps with 30 s per step using a thermal cycler.

366 Nucleic-acid scaffold (Table S1) for cryo-EM study of *E. coli* TTC-release was prepared as
367 follows: template-strand DNA (5'-GGGTATTGCGCGTGAATAAAAAGGGTACGCC-3';
368 0.39 mM, final concentration; Sangon Biotech) and RNA (5'- Cy5-ACGCGUCGCAGGCCU
369 UUUUAUU-3'; 0.3 mM, final concentration; GenScript Biotech Corp.) in 50 μ L annealing
370 buffer (5 mM Tris-HCl, pH 8.0, 200 mM NaCl, and 10 mM MgCl₂) were heated for 5 min at
371 95°C, cooled to 22 °C in 2 °C steps with 30 s per step using a thermal cycler.

372 For experiments shown in Figs 3G, S3, and S8C, DNA and RNA oligos (Table S1; Fig. S8C)
373 were obtained from Integrated DNA Technologies (IDT; Coralville, IA) and were purified by
374 denaturing polyacrylamide gel electrophoresis (PAGE; 15% 19:1 acrylamide: bisacrylamide,
375 45 mM Tris-borate, pH 8.3, 1.25 mM Na₂EDTA, 8M urea) before use, unless otherwise
376 stated. [γ -³²P]ATP, [α -³²P]UTP and [α -³²P]GTP were obtained from PerkinElmer Life
377 Sciences; rNTPs, from Promega (Madison, WI, USA); and 3'deoxy GTP (3'dGTP) from Jena
378 Bioscience.

379

380 **Cryo-EM data collection and processing: *E. coli* TTC-pause**

381 *E. coli* RNAP core enzyme (20 μ M, final concentration) and the nucleic-acid scaffold (26 μ M,
382 final concentration) were incubated in 0.5 mL 10 mM HEPES, pH 7.5, 5 mM KCl, 5 mM
383 MgCl₂, 3 mM DTT at room temperature for 50 min. The mixture was applied to a Superdex
384 200 10/300 column (Cytiva) equilibrated in 10 mM HEPES, pH 7.5, 5 mM KCl, 5 mM
385 MgCl₂, 3 mM DTT. Fractions containing TTC-pause complex were collected and
386 concentrated to 13 mg/mL.

387 The freshly purified *E. coli* TTC-pause at 13 mg/mL was incubated with 3-([3-
388 cholamidopropyl] dimethylammonio)-2-hydroxy-1-propanesulfonate (CHAPSO, 8 mM, final
389 concentration; Hampton Research Inc.) prior to grid preparation. The complex (3 μ L) was
390 subsequently applied on a glow-discharged C-flat CF-1.2/1.3 400 mesh holey carbon grids
391 (Electron Microscopy Sciences), blotted with Vitrobot Mark IV (FEI), and plunge-frozen in
392 liquid ethane with 95% chamber humidity at 10 °C.

393 The data were collected on a 300 keV Titan Krios (FEI) equipped with a K2 Summit direct
394 electron detector (Gatan) at National Center for Protein Sciences Shanghai. A total of 1,796
395 images were recorded using the Serial EM⁴³ in super-resolution counting mode with a pixel
396 size of 1.0 Å, and a dose rate of 8 electrons/pixel/s. Movies were recorded at 200 ms/frame

397 for 7.6 s (38 frames total) and defocus range was varied between -1.2 μ m and -2.2 μ m.
398 Frames of individual movies were aligned using MotionCor2⁴⁴, and contrast-transfer-function
399 estimations were performed using CTFFIND4⁴⁵. About 1,000 particles were picked and
400 subjected to 2D classification in RELION 3.0⁴⁶. The resulting distinct two-dimensional
401 classes were served as templates for particle auto-picking and 203,216 particles were picked
402 out. The resulting particles were subjected to 2D classification in RELION 3.0 by specifying
403 100 classes⁴⁶. Poorly-populated classes were removed. We used a 50- \AA low-pass-filtered map
404 calculated from structure of *E. coli* RNAP core enzyme (PDB: 6ALF) as the starting reference
405 model for 3D classification (N=3). The final concentration maps calculated from 132,648
406 particles were obtained through 3D auto-refinement, CTF-refinement, Bayesian polishing,
407 and post-processing in RELION 3.0. Gold-standard Fourier-shell-correlation analysis
408 indicated a mean map resolution of 3.58 \AA (Fig. S1)
409 The model of RNAP core enzyme from the cryo-EM structure of *E. coli* TEC (PDB: 6ALF)
410 was manually fit into the cryo-EM density map using Chimera⁴⁷. Rigid body and real-space
411 refinement was performed in Coot⁴⁸ and Phenix⁴⁹.
412

413 **Cryo-EM data collection and processing: *E. coli* TTC-hairpin**

414 The freshly purified *E. coli* TTC-pause complex (13 mg/mL, 33 μ M, final concentration) and
415 antisense RNA (asRNA10, 330 μ M, final concentration) were incubated in 30 μ L 10 mM
416 HEPES, pH 7.5, 5 mM KCl, 5 mM MgCl₂, 3 mM DTT for 3 h at 4°C. The sample was
417 vitrified by the same procedure as the TTC-pause complex.
418 The data were collected on a 300 keV Titan Krios (FEI) equipped with a K2 Summit direct
419 electron detector (Gatan) at center of Electron Microscopy, Zhejiang University. A total of
420 3,888 images were recorded using the Serial EM⁴³ in counting mode with a pixel size of
421 1.307 \AA , and a dose rate of 9.9 electrons/pixel/s. Movies were recorded at 250 ms/frame for
422 10 s (40 frames total) and defocus range was varied between -1.8 μ m and -2.6 μ m. Frames of
423 individual movies were aligned using MotionCor2⁴⁴, and contrast-transfer-function
424 estimations were performed using CTFFIND4⁴⁵. About 1,548 particles were picked and
425 subjected to 2D classification in RELION 3.0⁴⁶. The resulting distinct two-dimensional
426 classes were served as templates and a total of 1,548 particles were picked out. The
427 resulting particles were subjected to 2D classification in RELION 3.0 by specifying 100
428 classes⁴⁶. Poorly-populated classes were removed. We used a 50- \AA low-pass-filtered map
429 calculated from structure of *E. coli* RNAP core enzyme¹⁸ (PDB: 6ALF) as the starting
430 reference model for 3D classification (N=4). Two same classes were combined and 360,313
431 particles were used for 3D auto-refinement. To resolve heterogeneity around RNA hairpin in
432 RNA exit channel, a soft mask that excludes RNA duplex and nearby protein regions (β'
433 ZBD, β' dock, β flap, β CTR) was generated in Chimera and RELION 3.0. The mask was
434 used to make a subtracted particle stack in RELION 3.0. The subtracted particles were
435 applied for masked 3D classification (N=6, without alignment), the best-resolved class
436 containing obvious RNA hairpin (293,294 particles) was used for 3D auto-refinement, CTF-
437 refinement and Bayesian polishing, Postprocessing. Gold-standard Fourier-shell-correlation
438 analysis indicated a mean map resolution of 3.05 \AA (Fig. S4). The structural model of RNAP
439 core enzyme from the cryo-EM structure of *E. coli* hisPEC (PDB: 6ASX) was manually fit
440 into the cryo-EM density map using Chimera⁴⁷. Rigid-body and real-space refinement was
441 performed in Coot⁴⁸ and Phenix⁴⁹.
442

443 **Cryo-EM data collection and processing: *E. coli* TTC-release**

444 *E. coli* RNAP core enzyme (20 μ M, final concentration) and nucleic-acid scaffold comprising
445 tDNA and RNA (30 μ M, final concentration) were incubated in 0.5 mL 10 mM HEPES, pH
446 7.5, 50 mM KCl, 5 mM MgCl₂, 3 mM DTT at room temperature for 30 min. The ntDNA (200
447 μ M, final concentration) was subsequently added and the mixture was further incubated at
448 room temperature for 30 min. The mixture was applied to a Superdex 200 10/300 column
449 (Cytiva) equilibrated in 10 mM HEPES, pH 7.5, 50 mM KCl, 5 mM MgCl₂, 3 mM DTT.
450 Fractions containing TTC-pause complex were collected and concentrated to 17 mg/mL (~43
451 μ M), then the sample mixed with CHAPSO (Hampton Research, Inc.) to a final concentration

452 8 mM, 430 μ M (final concentration) antisense RNA12 (asRNA12) was added and the
453 reaction was incubated for 3 min prior to grid preparation. The complex (3 μ L) was quickly
454 applied on a glow-discharged UltraAuFoil R1.2/1.3 300 mesh holey Au grids (Quantifoil
455 Micro Tools GmbH), blotted with Vitrobot Mark IV (FEI), and plunge-frozen in liquid ethane
456 with 100% chamber humidity at 22 °C.
457 The data were collected on a 300 keV Titan Krios (FEI) equipped with a K3 Summit direct
458 electron detector (Gatan) at National Center for Protein Sciences Shanghai. A total of 1,355
459 images were recorded using the EPU using super-resolution counting mode for 2.67 s
460 exposures in 40 frames to give a total dose of 49.65 electrons per \AA^2 with defocus range of -
461 1.2 to -2.2 μ m. Frames of individual movies were aligned using MotionCor2⁴⁴, and contrast-
462 transfer-function estimations were performed using CTFFIND4⁴⁵. About 1,000 particles were
463 picked and subjected to 2D classification in RELION 3.0⁴⁶. The resulting distinct two-
464 dimensional classes were served as templates for auto-picking and a total of 592,713 particles
465 were picked out. The resulting particles were subjected to 2D classification in RELION 3.0
466 by specifying 100 classes⁴⁶. Poorly-populated classes were removed. We used a 50- \AA low-
467 pass-filtered map calculated from TTC-hairpin map as the starting reference model for 3D
468 classification (N=6). Two classes were combined and 282,423 the particle numbers used for
469 3D auto-refinement. To resolve heterogeneity about the DNA and RNA in the main cleft, a
470 soft map that excludes the upstream dsDNA, the transcription bubble, the RNA-DNA hybrid,
471 the downstream dsDNA, and the β' clamp domain nearby was generated in Chimera and
472 RELION 3.0. The mask was used to make a subtracted particle stack in RELION 3.0. The
473 subtracted particles were applied for masked 3D classification (N=6, without alignment), the
474 3D class of TTC-release (54,309 particles) were used for 3D auto-refinement, CTF-
475 refinement and Bayesian polishing, Postprocessing. Gold-standard Fourier-shell-correlation
476 analysis indicated a mean map resolution of 3.48 \AA (map A in Fig. S6D). The structural model
477 of RNAP core enzyme from the cryo-EM structure of *E. coli* hisPEC (PDB: 6ASX) was
478 manually fit into the cryo-EM map using Chimera⁴⁷. Rigid body and real-space refinement
479 was performed in Coot⁴⁸ and Phenix⁴⁹. The other two major classes were also processed under
480 the similar procedure resulting in two maps at 3.40 \AA (map B and C in Fig. S6D), both of
481 which show little signal for the upstream dsDNA, the non-template ssDNA, and the ssRNA in
482 the RNA exit channel, although clear signals for the downstream dsDNA and the half-
483 translocated RNA-DNA hybrid. These features suggest that these two complexes were likely
484 not properly assembled during complex reconstitution.
485

486 **Fluorescence-detected RNA release assay**

487 To study asRNA-induced RNA release, *E. coli* RNAP core enzyme (200 nM, final
488 concentration) and TTC-release nucleic-acid scaffold (800 nM, final concentration)
489 comprising Cy5-labelled RNA and tDNA were incubated in 300 mL transcription buffer (50
490 mM Tris-HCl, pH 8.0, 50 mM KCl, 5 mM MgCl₂, 5 mM β -mercaptoethanol at room
491 temperature for 15 min. Then ntDNA (2 μ M, final concentration) was subsequently added and
492 the mixture was further incubated at room temperature for 15 min to form TTC-pause
493 complex. The complex was immobilized on 150 mL Ni-NTA agarose beads (smart-
494 lifesciences, Inc.) pre-washed with transcription buffer. The immobilized complex was
495 washed with 300 mL transcription buffer for three times. The reaction mixture was aliquoted
496 and each of the aliquot (70 μ L) was supplemented with 7 mL asRNA12 (final concentration:
497 1 μ M) to induce RNA release. For each of the aliquots, 20 mL reaction mixtures were taken
498 out as reference of total amount of nascent RNA. The resulting reaction mixtures (50 μ L)
499 were separated into supernatant and pellet fractions by centrifugation at specified time points.
500 Both the total and supernatant samples (20 mL) were mixed with 5 μ L loading buffer (8 M
501 urea, 20 mM EDTA, 0.025% xylene cyanol), 95 °C boiled for 5 min, and cooled down in ice
502 for 5 min. RNA were separated by 20% urea-polyacrylamide slab gels (19:1
503 acrylamide/bisacrylamide) in 90 mM Tris-borate, pH 8.0 and 0.2 mM EDTA and analyzed by
504 fluorescein scanning (Typhoon; GE Healthcare, Inc.).
505

506 **Release assay to measure RNA and DNA rates release during intrinsic termination**

507 The TTC release scaffold (Figure 3A) was modified by addition of 12 downstream base pairs
508 to eliminate any effect of RNAP–DNA-end contacts that could affect the DNA release rate
509 (Figure 3H). ECs were reconstituted one nucleotide upstream from the U8 termination site by
510 incubation of 1 μ M RNA21, 200 nM T DNA that was 5' 32 P-labeled by treatment with [γ -
511 32 P]ATP polynucleotide kinase, and 400 nM *E. coli* core RNAP in 100 μ L EC buffer (10 mM
512 Hepes, pH 8.0, 50 mM KGlutamate, 10 mM MgOAc, 0.1 mM EDTA, 5 μ g acetylated
513 BSA/mL and 1 mM DTT) for 5 min at 37 °C. Non-template DNA (2 μ M) was added and the
514 mixture was incubated for an additional 5 min at 37 °C. The final ratio of RNAP:RNA:T:NT
515 was 2:5:1:10. The estimated concentration of the assembled transcription termination
516 complex was 200 nM. Heparin (50 μ g/mL) was added to the mixture to prevent core RNAP
517 from rebinding to the scaffold after release. The RNA was extended to U8 by reaction with 2
518 μ M [α - 32 P]UTP (136 Ci/mmol) yielding TTC with 5' 32 P-labeled T DNA and 3' 32 P-labeled
519 RNA. The complex was immobilized on 20 μ L of Ni-NTA agarose beads (Qiagen) with
520 occasional pipetting. After 10 min incubation at room temperature, the immobilized complex
521 was washed with EC buffer (five cycles of centrifugation and resuspension of the pelleted
522 beads in 200 μ L of fresh EC buffer). The washed bead-complex was resuspended in 200 μ L
523 EC buffer. One 5 μ L portion was mixed with 5 μ L stop buffer (8 M urea, 50 mM EDTA, 90
524 mM Tris-Borate buffer, pH 8.3, 0.02% bromophenol blue, 0.02% xylene cyanol) for total 0-
525 timepoint sample. A second 5 μ L portion was incubated with ATP, CTP, and 3'-dGTP (150
526 μ M each), then combined with stop buffer as a check for TTC integrity. (Fig. 3H). The
527 magnetic Ni-NTA beads were pulled to one side using a magnet, then 25 μ L of the
528 supernatant was passed through a nitrocellulose microfilter plate (384 wells) placed on top of
529 a multi-well plate vacuum manifold (Operated at 20 Hg) with a receiver plate on the bottom
530 (Pall Corporation). A portion (5 μ L) of the filtrate was mixed with 5 μ L stop buffer for the
531 released 0-timepoint sample. To initiate the termination reaction and monitor RNA and DNA
532 release, asRNA – 12mer (Fig. 3H) was added to a final concentration of 1 μ M and supernatant
533 portions (25 μ L) were removed after 10, 20, 30, 60, 120 and 180 s, filtered, and combined
534 with stop buffer as described for the 0-timepoint sample. Samples were then analyzed by
535 denaturing PAGE (15% 19:1 acrylamide: bis-acrylamide, 45 mM Tris-borate, pH 8.3, 1.25
536 mM Na₂EDTA, 8M urea) for 2 h at 60 W, the gel exposed on a Storage Phosphor Screen and
537 imaged on a Typhoon PhosphoImager (GE Healthcare). The RNA and T DNA were quantified
538 using Image J software (NIH). Released RNA and DNA were compared to the total samples
539 to calculate fractions remaining in the TTC from triplicate reactions. These fractions vs. time
540 were fit to a first-order dissociation rate equation with a small fraction that remained bound to
541 the beads (recalcitrant to release) (Fig. 3H). The recalcitrant fractions (both RNA and DNA)
542 were 0.05 for the first replicate and 0.13 for the second and third replicates. One timepoint
543 (30 s) was lost for replicate 1.

544

545 ***In vitro* transcription assay**

546 DNA templates used for in vitro transcription assays contains the T5-N25 promoter, a coding
547 region, and the λ_{R2} terminator. The DNA template was prepared by PCR primer extension
548 using the single-stranded ntDNA (5'-TCATAAAAAATTATTGCTTCAGGAAAATT
549 TCTGTATAATAGATTCTAAATTGAGAGAGGAGTTAAATCCAGGCCTGCTGGTAA
550 TCGCAGGCCTTTATTGGATCCCCGGGTAGAATTG-3'; 1 μ M; RuiMian) as
551 template and tDNA (5'- CGAATTCTACCCGGGGATCCAAATAAAAGGCCTGCGATT
552 ACCAGCAGGCCTGGATT TA TGATCCCCGAGGAGAAGCAGAGGTACC-3'; 2 μ M;
553 Sangon Biotech) as the primer in a thermal cycler. The efficiency of primer extension was
554 confirmed on a 1.5% agarose gel and the extended dsDNA were further purified by a Gel
555 Extraction Kit (Omega Bio-Tek). The pre-melted DNA templates were prepared by the same
556 procedure using tDNA primer with non-complementary sequences at the specified positions
557 (Figs 3G, S8A, and S8B).

558 Reaction mixture (20 μ L) in transcription buffer (40 mM Tris-HCl, pH 8.0, 75 mM NaCl, 5
559 mM MgCl₂, 12.5% Glycerol, 2.5 mM DTT, and 50 μ g/ml BSA) containing RNAP holo-
560 enzyme (50 nM) and DNA template (50 nM) were incubated for 10 min at 37 °C. RNA

561 synthesis was initiated by addition of 1.2 μ L NTP mixture (5 μ M ATP, 5 μ M GTP, 0.05 μ M
562 UTP and 0.55 μ M [α - 32 P]UTP (45 Bq/fmol), final concentration) for 10 min at 37 °C to obtain
563 TECs halted at U25. Subsequently, 1 μ L Heparin (50 μ g/mL; final concentration) was added
564 to only allows single-round transcription. RNA extension was resumed by addition of 1 μ L
565 NTP mixture (5 μ M ATP, 5 μ M CTP, 5 μ M GTP, and 5 μ M UTP; final concentration).
566 Reactions were terminated by adding 5 μ L loading buffer, boiled at 95 °C for 5 min, and
567 cooled down in ice for 5 min. The RNA transcripts were separated by 12% urea-
568 polyacrylamide slab gels (19:1 acrylamide/bisacrylamide) in 90 mM Tris-borate, pH 8.0 and
569 0.2 mM EDTA and analyzed by storage-phosphor scanning (Typhoon; GE Healthcare, Inc.).
570 Promoter-based template DNA sequences with a λ P_R promoter, C-less cassette, and wild-type
571 or variant λ t_{R2} or ft₅₀₀ terminators for experiments shown in Figs. S3 and S8C were PCR-
572 amplified using primers flanking both ends and gel-purified using Qiagen Qiaquick
573 purification reagents. NusA protein was purified as described previously⁵⁰. Core RNAP was
574 incubated with σ ⁷⁰ for 30 min at 37 °C to form holo-RNAP. To initiate transcription, holo-
575 RNAP (31.25 nM) was incubated with template DNA (25 nM), ApU (150 μ M), ATP + UTP
576 (both at 2.5 μ M), and 2 μ M [α - 32 P]GTP (54.5 Ci/mmol) in EC buffer (10 mM Hepes, pH 8.0,
577 50 mM KGlutamate, 10 mM MgOAc, 0.1 mM EDTA, 5 μ g acetylated BSA/mL and 1 mM
578 DTT) for 5 min at 37 °C to form a halted complex at A26. Transcription was then restarted by
579 adding a mastermix containing NTP mix (A+C+G+U), Heparin and KGlutamate at a final
580 concentration of 150 μ M, 50 μ g/mL and 100 mM respectively. Reactions were stopped and
581 products were separated as described above. The termination efficiencies were calculated
582 from three independent replicates.
583 For experiments shown in Fig. S3F, ECs were reconstituted 15 nucleotides upstream from the
584 U8 termination site by incubation of 25 nM RNA23, 50 nM T DNA, and 50 nM *E. coli* core
585 RNAP in 50 μ L EC buffer (10 mM Hepes, pH 8.0, 50 mM KGlutamate, 10 mM MgOAc, 0.1
586 mM EDTA, 5 μ g/mL Acetylated BSA and 1 mM DTT) for 5 min at 37 °C. Non-template
587 DNA (125 nM) was added and the mixture was incubated for an additional 5 min at 37 °C.
588 Heparin (50 μ g/mL) was added to the mixture to prevent core RNAP from rebinding to
589 nucleic acids. The RNA was extended to A25 by a reaction with ATP + CTP (2.5 μ M final for
590 both) followed by radiolabeling to G27 by reacting with 0.037 μ M [α - 32 P]GTP (3000
591 Ci/mmol). The RNA was then extended to the termination site by addition of 150 μ M NTP
592 mix.

593

594 **Data availability**

595 The cryo-EM map and coordinates were deposited in Protein Data Bank and Electron
596 Microscopy Data Bank (TTC-pause: 7YP9 and EMD-33996; TTC-hairpin: 7YPA, EMD-33997;
597 TTC-release: 7YPB, EMD-33998).

598

599

600

601

602

603

604

605

606

607

608

609

610

611

612

613 **References**

614 1 Vannini, A. & Cramer, P. Conservation between the RNA polymerase I, II, and III
615 transcription initiation machineries. *Mol Cell* **45**, 439-446,
616 doi:10.1016/j.molcel.2012.01.023 (2012).

617 2 Porrua, O. & Libri, D. Transcription termination and the control of the transcriptome:
618 why, where and how to stop. *Nat Rev Mol Cell Biol* **16**, 190-202,
619 doi:10.1038/nrm3943 (2015).

620 3 Ray-Soni, A., Bellecourt, M. J. & Landick, R. Mechanisms of Bacterial Transcription
621 Termination: All Good Things Must End. *Annu Rev Biochem* **85**, 319-347,
622 doi:10.1146/annurev-biochem-060815-014844 (2016).

623 4 Proudfoot, N. J. Transcriptional termination in mammals: Stopping the RNA
624 polymerase II juggernaut. *Science* **352**, aad9926, doi:10.1126/science.aad9926
625 (2016).

626 5 Roberts, J. W. Mechanisms of Bacterial Transcription Termination. *J Mol Biol* **431**,
627 4030-4039, doi:10.1016/j.jmb.2019.04.003 (2019).

628 6 Arimbasseri, A. G. & Maraia, R. J. Mechanism of Transcription Termination by RNA
629 Polymerase III Utilizes a Non-template Strand Sequence-Specific Signal Element.
630 *Mol Cell* **58**, 1124-1132, doi:10.1016/j.molcel.2015.04.002 (2015).

631 7 Nielsen, S., Yuzenkova, Y. & Zenkin, N. Mechanism of eukaryotic RNA polymerase
632 III transcription termination. *Science* **340**, 1577-1580, doi:10.1126/science.1237934
633 (2013).

634 8 Yarnell, W. S. & Roberts, J. W. Mechanism of intrinsic transcription termination and
635 antitermination. *Science* **284**, 611-615 (1999).

636 9 Mairhofer, J., Wittwer, A., Cserjan-Puschmann, M. & Striedner, G. Preventing T7
637 RNA polymerase read-through transcription-A synthetic termination signal capable of
638 improving bioprocess stability. *ACS Synth Biol* **4**, 265-273, doi:10.1021/sb5000115
639 (2015).

640 10 Peters, J. M., Vangeloff, A. D. & Landick, R. Bacterial transcription terminators: the
641 RNA 3'-end chronicles. *J Mol Biol* **412**, 793-813, doi:10.1016/j.jmb.2011.03.036
642 (2011).

643 11 Chen, Y. J. *et al.* Characterization of 582 natural and synthetic terminators and
644 quantification of their design constraints. *Nat Methods* **10**, 659-664,
645 doi:10.1038/nmeth.2515 (2013).

646 12 Gusarov, I. & Nudler, E. The mechanism of intrinsic transcription termination. *Mol*
647 *Cell* **3**, 495-504 (1999).

648 13 Kang, J. Y. *et al.* RNA Polymerase Accommodates a Pause RNA Hairpin by Global
649 Conformational Rearrangements that Prolong Pausing. *Mol Cell* **69**, 802-815 e801,
650 doi:10.1016/j.molcel.2018.01.018 (2018).

651 14 Guo, X. *et al.* Structural Basis for NusA Stabilized Transcriptional Pausing. *Mol Cell*
652 **69**, 816-827 e814, doi:10.1016/j.molcel.2018.02.008 (2018).

653 15 Vos, S. M., Farnung, L., Urlaub, H. & Cramer, P. Structure of paused transcription
654 complex Pol II-DSIF-NELF. *Nature* **560**, 601-606, doi:10.1038/s41586-018-0442-2
655 (2018).

656 16 Vvedenskaya, I. O. *et al.* Interactions between RNA polymerase and the "core
657 recognition element" counteract pausing. *Science* **344**, 1285-1289,
658 doi:10.1126/science.1253458 (2014).

659 17 Larson, M. H. *et al.* A pause sequence enriched at translation start sites drives
660 transcription dynamics *in vivo*. *Science* **344**, 1042-1047,
661 doi:10.1126/science.1251871 (2014).

662 18 Kang, J. Y. *et al.* Structural basis of transcription arrest by coliphage HK022 Nun in
663 an Escherichia coli RNA polymerase elongation complex. *eLife* **6**,
664 doi:10.7554/eLife.25478 (2017).

665 19 Zhu, C. *et al.* Transcription factors modulate RNA polymerase conformational
666 equilibrium. *Nat Commun* **13**, 1546, doi:10.1038/s41467-022-29148-0 (2022).

667 20 Yang, Y. *et al.* Structural visualization of transcription activated by a multidrug-
668 sensing MerR family regulator. *Nat Commun* **12**, 2702, doi:10.1038/s41467-021-
669 22990-8 (2021).

670 21 Lubkowska, L., Maharjan, A. S. & Komissarova, N. RNA folding in transcription
671 elongation complex: implication for transcription termination. *J Biol Chem* **286**,
672 31576-31585, doi:10.1074/jbc.M111.249359 (2011).

673 22 King, R. A., Markov, D., Sen, R., Severinov, K. & Weisberg, R. A. A conserved zinc
674 binding domain in the largest subunit of DNA-dependent RNA polymerase modulates
675 intrinsic transcription termination and antitermination but does not stabilize the
676 elongation complex. *J Mol Biol* **342**, 1143-1154, doi:10.1016/j.jmb.2004.07.072
677 (2004).

678 23 Toulokhonov, I. & Landick, R. The flap domain is required for pause RNA hairpin
679 inhibition of catalysis by RNA polymerase and can modulate intrinsic termination.
680 *Mol Cell* **12**, 1125-1136, doi:10.1016/s1097-2765(03)00439-8 (2003).

681 24 Ray-Soni, A., Mooney, R. A. & Landick, R. Trigger loop dynamics can explain
682 stimulation of intrinsic termination by bacterial RNA polymerase without terminator
683 hairpin contact. *Proc Natl Acad Sci U S A* **114**, E9233-E9242,
684 doi:10.1073/pnas.1706247114 (2017).

685 25 Komissarova, N., Becker, J., Solter, S., Kireeva, M. & Kashlev, M. Shortening of
686 RNA:DNA hybrid in the elongation complex of RNA polymerase is a prerequisite for
687 transcription termination. *Mol Cell* **10**, 1151-1162 (2002).

688 26 Larson, M. H., Greenleaf, W. J., Landick, R. & Block, S. M. Applied force reveals
689 mechanistic and energetic details of transcription termination. *Cell* **132**, 971-982,
690 doi:10.1016/j.cell.2008.01.027 (2008).

691 27 Santangelo, T. J. & Roberts, J. W. Forward translocation is the natural pathway of
692 RNA release at an intrinsic terminator. *Mol Cell* **14**, 117-126 (2004).

693 28 Epshteyn, V., Cardinale, C. J., Ruckenstein, A. E., Borukhov, S. & Nudler, E. An
694 allosteric path to transcription termination. *Mol Cell* **28**, 991-1001,
695 doi:10.1016/j.molcel.2007.10.011 (2007).

696 29 Kashlev, M. & Komissarova, N. Transcription termination: primary intermediates and
697 secondary adducts. *J Biol Chem* **277**, 14501-14508, doi:10.1074/jbc.M200215200
698 (2002).

699 30 Bellecourt, M. J., Ray-Soni, A., Harwig, A., Mooney, R. A. & Landick, R. RNA
700 Polymerase Clamp Movement Aids Dissociation from DNA but Is Not Required for
701 RNA Release at Intrinsic Terminators. *J Mol Biol* **431**, 696-713,
702 doi:10.1016/j.jmb.2019.01.003 (2019).

703 31 Park, J. S. & Roberts, J. W. Role of DNA bubble rewinding in enzymatic transcription
704 termination. *Proc Natl Acad Sci U S A* **103**, 4870-4875,
705 doi:10.1073/pnas.0600145103 (2006).

706 32 Ryder, A. M. & Roberts, J. W. Role of the non-template strand of the elongation
707 bubble in intrinsic transcription termination. *J Mol Biol* **334**, 205-213,
708 doi:10.1016/j.jmb.2003.09.039 (2003).

709 33 Shankar, S., Hatoum, A. & Roberts, J. W. A transcription antiterminator constructs a
710 NusA-dependent shield to the emerging transcript. *Mol Cell* **27**, 914-927 (2007).

711 34 Harden, T. T. *et al.* Alternative transcription cycle for bacterial RNA polymerase. *Nat Commun* **11**, 448, doi:10.1038/s41467-019-14208-9 (2020).

712 35 Kang, W. *et al.* Transcription reinitiation by recycling RNA polymerase that diffuses on DNA after releasing terminated RNA. *Nat Commun* **11**, 450, doi:10.1038/s41467-019-14200-3 (2020).

713 36 Pei, H. H. *et al.* The delta subunit and NTPase HelD institute a two-pronged mechanism for RNA polymerase recycling. *Nat Commun* **11**, 6418, doi:10.1038/s41467-020-20159-3 (2020).

714 37 Kouba, T. *et al.* Mycobacterial HelD is a nucleic acids-clearing factor for RNA polymerase. *Nat Commun* **11**, 6419, doi:10.1038/s41467-020-20158-4 (2020).

715 38 Newing, T. P. *et al.* Molecular basis for RNA polymerase-dependent transcription complex recycling by the helicase-like motor protein HelD. *Nat Commun* **11**, 6420, doi:10.1038/s41467-020-20157-5 (2020).

716 39 Hou, H. *et al.* Structural insights into RNA polymerase III-mediated transcription termination through trapping poly-deoxythymidine. *Nat Commun* **12**, 6135, doi:10.1038/s41467-021-26402-9 (2021).

717 40 M., G. *et al.* Architecture of the yeast Pol III pre-termination complex and pausing mechanism on poly-dT termination signals. *bioRxiv*, doi:10.1101/2022.02.28.482286 (2022).

718 41 Hudson, B. P. *et al.* Three-dimensional EM structure of an intact activator-dependent transcription initiation complex. *Proc Natl Acad Sci U S A* **106**, 19830-19835, doi:10.1073/pnas.0908782106 (2009).

719 42 Hein, P. P. *et al.* RNA polymerase pausing and nascent-RNA structure formation are linked through clamp-domain movement. *Nat Struct Mol Biol* **21**, 794-802, doi:10.1038/nsmb.2867 (2014).

720 43 Mastronarde, D. N. Automated electron microscope tomography using robust prediction of specimen movements. *J Struct Biol* **152**, 36-51, doi:10.1016/j.jsb.2005.07.007 (2005).

721 44 Zheng, S. Q. *et al.* MotionCor2: anisotropic correction of beam-induced motion for improved cryo-electron microscopy. *Nat Methods* **14**, 331-332, doi:10.1038/nmeth.4193 (2017).

742 45 Rohou, A. & Grigorieff, N. CTFFIND4: Fast and accurate defocus estimation from
743 electron micrographs. *J Struct Biol* **192**, 216-221, doi:10.1016/j.jsb.2015.08.008
744 (2015).

745 46 Zivanov, J. *et al.* New tools for automated high-resolution cryo-EM structure
746 determination in RELION-3. *Elife* **7**, doi:10.7554/eLife.42166 (2018).

747 47 Pettersen, E. F. *et al.* UCSF Chimera--a visualization system for exploratory research
748 and analysis. *J. Comput. Chem.* **25**, 1605-1612, doi:10.1002/jcc.20084 (2004).

749 48 Emsley, P. & Cowtan, K. Coot: model-building tools for molecular graphics. *Acta
750 Crystallogr D Biol Crystallogr* **60**, 2126-2132, doi:10.1107/S0907444904019158
751 (2004).

752 49 Adams, P. D. *et al.* PHENIX: a comprehensive Python-based system for
753 macromolecular structure solution. *Acta Crystallogr D Biol Crystallogr* **66**, 213-221,
754 doi:10.1107/S0907444909052925 (2010).

755 50 Ha, K. S., Toulokhonov, I., Vassylyev, D. G. & Landick, R. The NusA N-terminal
756 domain is necessary and sufficient for enhancement of transcriptional pausing via
757 interaction with the RNA exit channel of RNA polymerase. *J Mol Biol* **401**, 708-725,
758 doi:10.1016/j.jmb.2010.06.036 (2010).

759

760 Acknowledgments

761 The Work was supported by the Basic Research Zone Program of Shanghai JCYJ-SHFY-
762 2022-012 (YZ), National Key Research and Development Program of China
763 2018YFA0900701 (Y.Z.), Strategic Priority Research Program of the CAS XDB29020000
764 (Y.Z.), and US National Institute of General Medical Sciences, NIH (GM38660) (R.L.).
765 We thank Dr. Liangliang Kong, Dr. Fangfang Wang, Dr. Guangyi Li, and Dr. Jialin Duan at
766 the cryo-EM center of NFPS in Shanghai, Dr. Shenghai Chang at the cryo-EM center of
767 Zhejiang University.

768

769 Author contributions

770 L.Y. collected the cryo-EM data, solved the cryo-EM structures. L.Y., E.O., C.Y. and R.M.
771 performed biochemical experiments. S.J., L.S., X.W., D.H., Y.Z. and Y.F. assisted in structure
772 determination. R.L. and Y.Z. designed experiments, analyzed data, and wrote the manuscript.

773

774 Competing interests

775 Authors declare that they have no competing interests.

776

777 Materials & Correspondence

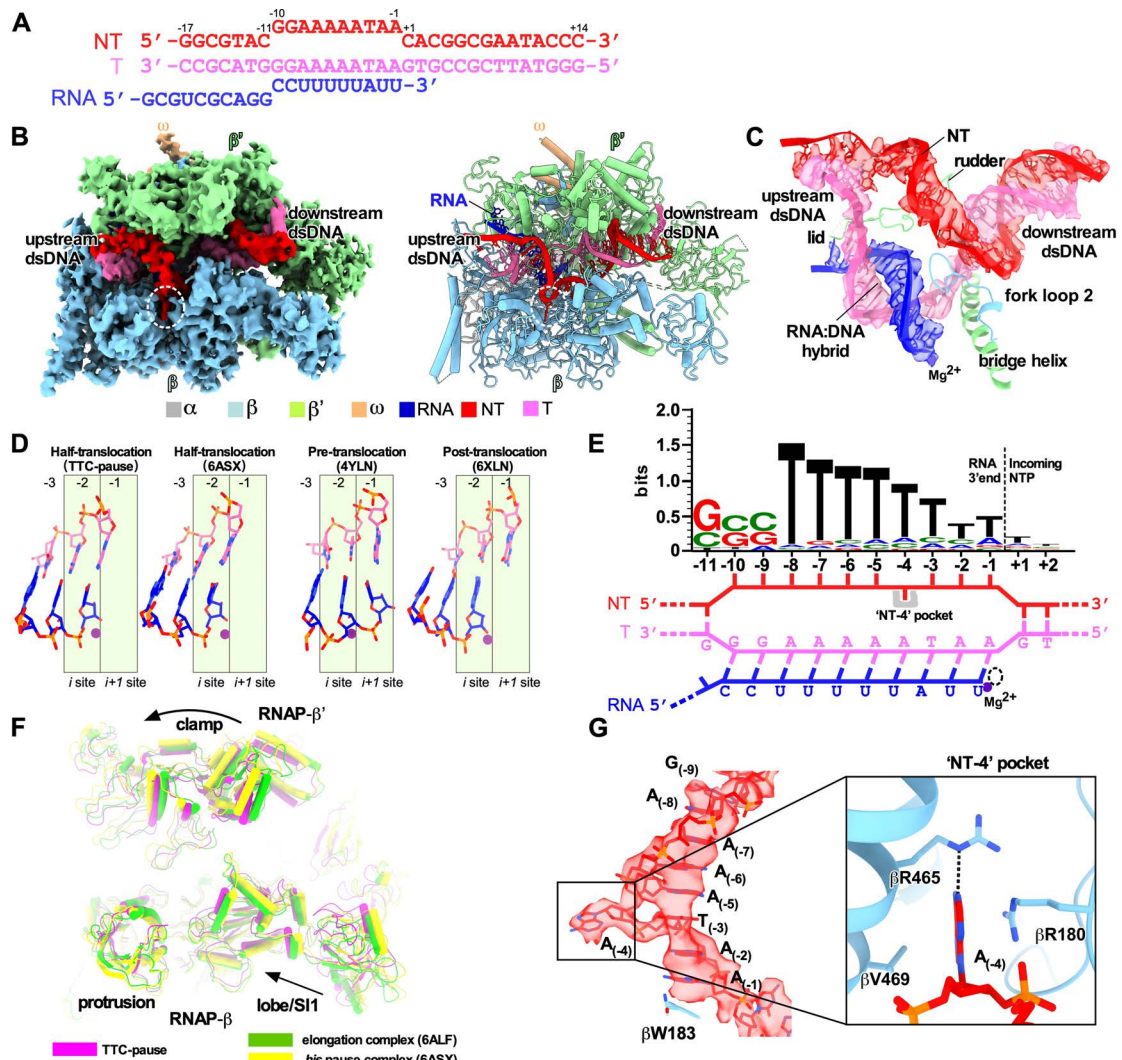
778 Correspondence and requests for materials should be addressed to Y.Z.
779 (yzhang@cemps.ac.cn) or R.L. (rlandick@wisc.edu).

780

781

782

783 **Figures and figure legends**



784

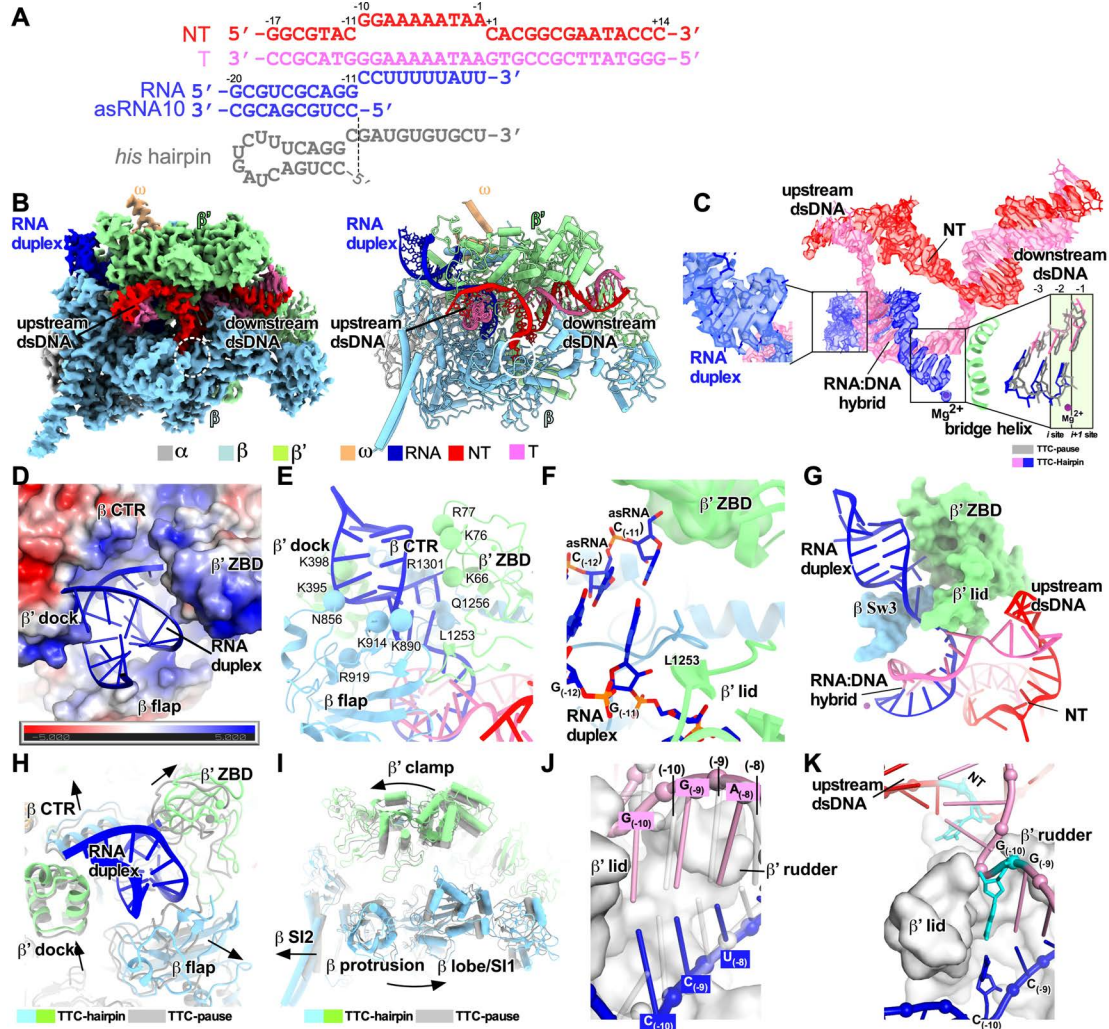
785

Figure 1. The TTC-pause complex. (A) The sequences of the nucleic-acid scaffold used for cryo-EM study. **(B)** The cryo-EM map (left) and structural model (right) for TTC-pause complex. The RNAP subunits and nucleic-acid chains are colored as in the color scheme. **(C)** The cryo-EM map for the nucleic-acid scaffold. **(D)** The comparison of the RNA-DNA translocation states among TTC-pause complex, half-translocation state in a hairpin-stabilized paused transcription elongation complex (*hisPEC*; PDB: 6ASX), a pre-translocation complex (PDB: 4YLN), and a post-translocation complex (PDB: 6XLN). **(E)** The consensus sequence of bacterial intrinsic terminators (upper panel)¹¹ and the schematic presentation of the nucleotides of the transcription bubble in the TTC-pause complex. **(F)** The conformational comparison among TTC-pause complex, TEC (PDB: 6ALF), and *hisPEC* (PDB: 6ASX). **(G)** The cryo-EM map and structural model of ntDNA of the transcription bubble. The insert shows the interaction between the flipped $A_{(-4)}$ nucleotide and the 'NT-4' pocket.

796

797

798



799

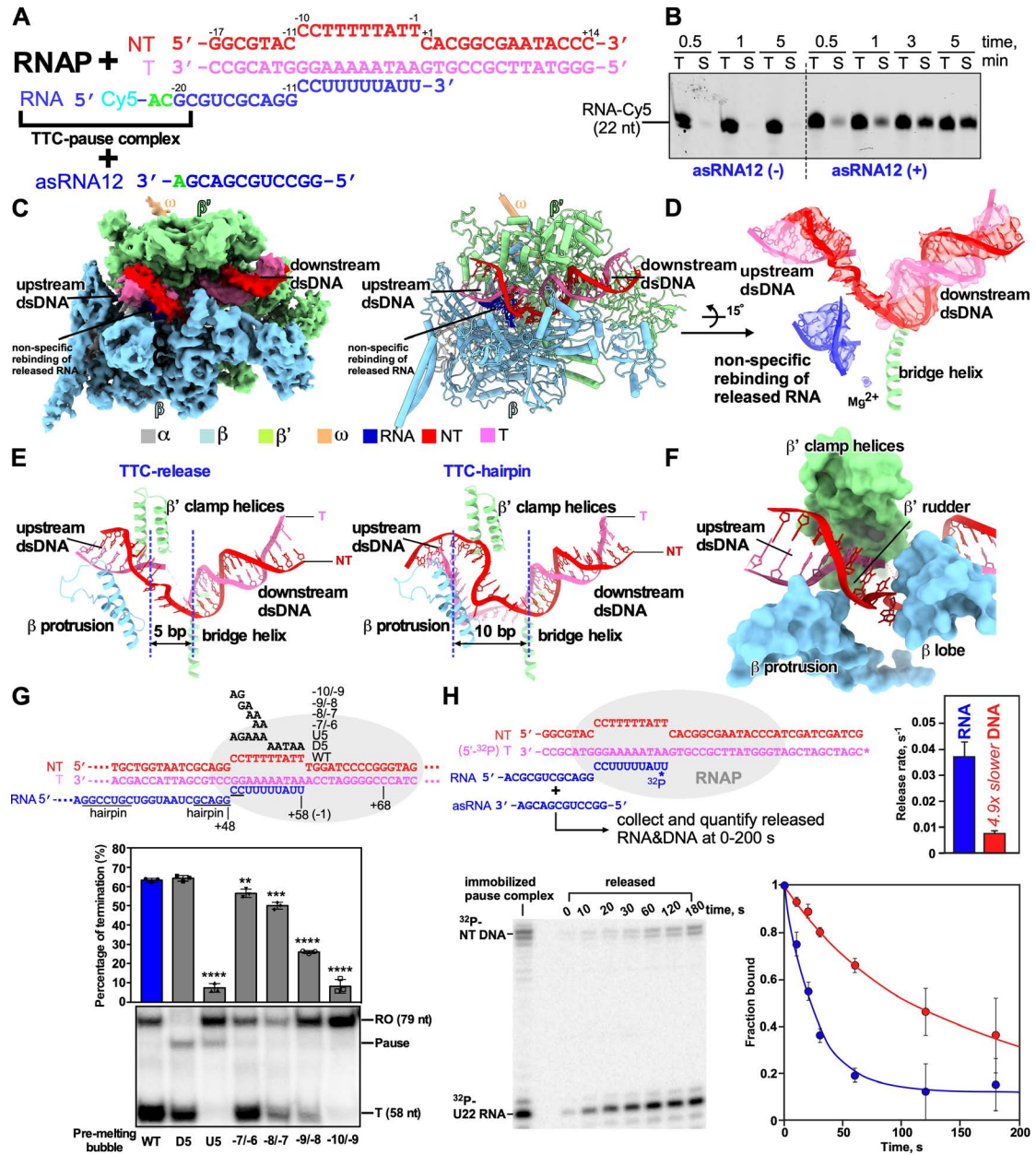
800

Figure 2. The TTC-hairpin complex. (A) The nucleic-acid scaffold and the antisense RNA (asRNA) used for cryo-EM structure determination. **(B)** The cryo-EM map (left) and structural model (right) for TTC-hairpin complex. **(C)** The cryo-EM map for nucleic-acid scaffold. The left insert shows the map for the RNA duplex in the RNA exit channel and the right insert shows the superimposition of the base pairs (-3 to 1) of the RNA-DNA hybrid between TTC-hairpin (colored as in the scheme) and TTC-pause (gray). **(D)** RNA duplex in the RNA exit channel. The electrostatic potential surface of RNAP was generated using APBS tools in Pymol. **(E)** The detailed interaction of the RNA duplex with residues in the RNA exit channel. Spheres, the C α atom of polar residues in H-bond distance with the phosphate backbone of RNA duplex. **(F)** The interaction of the -11 base pair of RNA duplex with residues in the RNA exit channel. **(G)** Further extension of RNA duplex is blocked by RNAP β' ZBD, β' lid, and β Sw3 motifs. **(H)** The structural comparison of RNA exit channel between TTC-pause (gray) and TTC-hairpin (colored). **(I)** The global conformational movement of TTC-hairpin (colored) compared with TTC-pause (gray). **(J)** The comparison of the first three base pairs of the RNA-DNA hybrid between TTC-hairpin (pink and blue) and TEC (gray) (PDB: 6ALF). The two structures were superimposed based in the RNAP- β' lid and rudder motifs. **(K)** The $G_{(-10)}$ of the tDNA is under the tunnel formed by RNAP- β' lid and rudder and ready to pair with the -10 nucleotide of ntDNA.

819

820

821

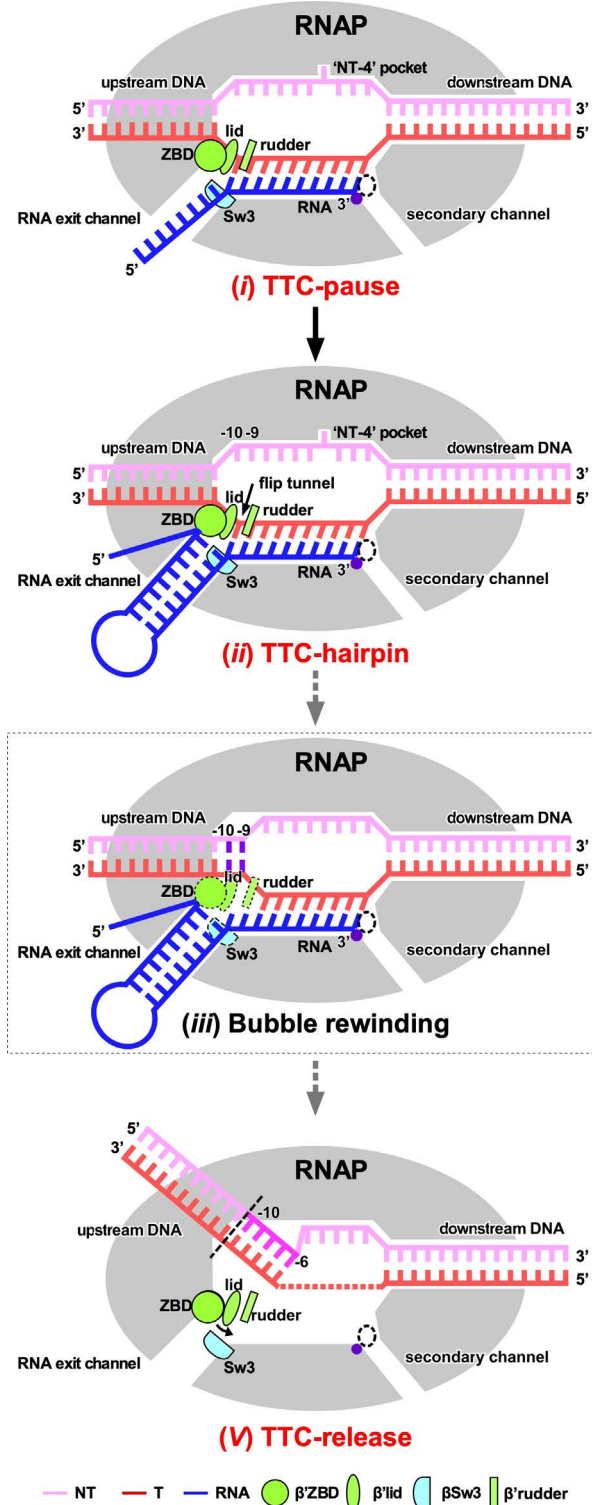


822
823

Figure 3 The release complex of transcription termination. (A) The asRNA-induced termination strategy used for obtaining the cryo-EM structure of TTC-release. **(B)** The results of RNA release assay show that asRNA12 induces release of nascent RNA in a time-dependent manner. T, total fraction; S, supernatant fraction. **(C)** The cryo-EM map and structural model of TTC-release. **(D)** The cryo-EM map and model of the nucleic-acid scaffold TTC-release. **(E)** The comparison of transcription bubble sizes of TTC-release and TTC-hairpin. **(F)** The rewound 5-bp dsDNA (-10 to -6) were loosely restrained by β protrusion, β' clamp helices, and β' rudder and further rewinding of the upstream dsDNA is stopped by the β lobe domain due to a closed clamp. **(G)** The *in vitro* transcription assay suggests that DNA unwinding is required for intrinsic termination at the λ-tR2 terminator. Data are presented as mean ± SEM, n=3 biologically independent experiments. **P<0.01, ***P<0.001, ****P<0.0001. **(H)** RNA releases from TTC during termination faster than DNA releases. A TTC scaffold making all RNAP contacts with ³²P label on the T strand 5' O and RNA 3' phosphodiester was immobilized on beads. Upon asRNA addition, the rate of RNA release was $0.037 \pm 0.006 \text{ s}^{-1}$ whereas DNA released at $0.0075 \pm 0.001 \text{ s}^{-1}$.

839
840

841



842

843

844 **Figure 4 The proposed pathway of intrinsic termination.** Intermediate states confirmed by
845 structures obtained in this study are labeled in red text. A proposed intermediate state in the
846 pathway is labeled in black text and boxed by dotted lines. See also Fig. S9.

847

848

849

850